DIGITAL ACCESS TO SCHOLARSHIP AT HARVARD
DASH.HARVARD.EDU

HARVARD LIBRARY
Office for Scholarly Communication

Extrusion, slide, and rupture of an elastomeric seal

Citation
Wang, Zhengjin, Chao Chen, Qihan Liu, Yucun Lou, and Zhigang Suo. 2017. Extrusion, Slide, and Rupture of an Elastomeric Seal. Journal of the Mechanics and Physics of Solids 99: 289–303. doi:10.1016/j.jmps.2016.12.007.

Published Version
doi:10.1016/j.jmps.2016.12.007

Permanent link
http://nrs.harvard.edu/urn-3:HUL.InstRepos:29995315

Terms of Use
This article was downloaded from Harvard University's DASH repository, and is made available under the terms and conditions applicable to Open Access Policy Articles, as set forth at http://nrs.harvard.edu/urn-3:HUL.InstRepos:dash.current.terms-of-use#OAP

Share Your Story

The Harvard community has made this article openly available.
Please share how this access benefits you. Submit a story .

Accessibility

Extrusion, slide, and rupture of an elastomeric seal

Zhengjin Wang[1,2*], Chao Chen[1*], Qihan Liu[1], Yucun Lou[3], Zhigang Suo[1(a)]

[1] John A. Paulson School of Engineering and Applied Sciences, Kavli Institute for Nanobio Science and Technology, Harvard University, Cambridge, MA 02138, USA

[2] State Key Lab for Strength and Vibration of Mechanical Structures, International Center for Applied Mechanics, School of Aerospace Engineering, Xi'an Jiaotong University, Xi'an 710049, China

[3] Schlumberger-Doll Research, One Hampshire Street, Cambridge, MA 02139, USA

*These authors contributed equally to this work.

(a) Email: suo@seas.harvard.edu

Abstract. Elastomeric seals are essential to two great technological advances in oilfields: horizontal drilling and hydraulic fracturing. This paper describes a method to study elastomeric seals by using the pressure-extrusion curve (i.e., the relation between the drop of pressure across a seal and the volume of extrusion of the elastomer). Emphasis is placed on a common mode of failure found in oilfields: leak caused by a crack across the length of a long seal. We obtain an analytical solution of large elastic deformation, which is analogous to the Poiseuille flow of viscous liquids. We further obtain analytical expressions for the energy release rate of a crack and the critical pressure for the onset of its propagation. The theory predicts the pressure-extrusion curve using material parameters (elastic modulus, sliding stress, and fracture energy) and geometric parameters (thickness, length, and precompression). We fabricate seals of various parameters in transparent chambers on a desktop, and watch the seals extrude, slide, rupture and leak. The experimentally measured pressure-extrusion curves agree with theoretical predictions remarkably well.

Keywords: Seal; Large deformation; Friction; Fracture; Leak.

1. Introduction

Seals—along with tires, bearings, and medical gloves—are among the most significant applications of elastomers (Gent, 2012). In daily life, elastomeric seals are ubiquitous in plumbing joints, bottle caps, and pressure cookers. In engines and hydraulics, elastomeric seals enable fluid-tight, reciprocating motion of pistons in cylinders (Nau, 1999). Attributes of elastomeric seals include high sealing pressure, light weight, and low cost. Elastomeric seals are inexpensive, but their failure can be costly. The explosion of the space shuttle Challenger, for example, was traced to the failure of an O-ring (Rogers et al., 1986).

Our own interest focuses on elastomeric seals used in the oil and gas industry. These seals are commonly known as packers, and are used to isolate fluids in gaps between pipes and boreholes (Al Douseri et al., 2009; Ezeukwu et al., 2007; Kleverlaan et al., 2005). The packers achieve sealing either by mechanical mechanisms (mechanical packers) (Coronado et al., 2002), or by imbibing fluids (swellable packers) (Cai et al., 2010; Druecke et al., 2015; Lou and Chester, 2014). Seals are essential to the two great technological advances in oilfields: horizontal drilling and hydraulic fracturing (Davis and McCrady, 2008; Gavioli and Vicario, 2012; Miller et al., 2015; Yakeley et al., 2007).

Elastomers can sustain essentially arbitrarily high pressure, so long as the pressure has the same magnitude in all directions and in all places (i.e., hydrostatic and homogeneous pressure). The function of a seal, however, is to sustain a *drop of pressure*. The inhomogeneous pressure inevitably leads to shear and tensile stress, which causes the elastomer to deform and possibly rupture. When a seal is used to enable hydraulic fracturing, the pressure at one end of the seal must be high enough to fracture rocks, and the pressure at the other end of the seal can be as low as that in the ambient. These requirements correspond to a drop of pressure up to 70 MPa (Nijhof et al., 2010). Such a large drop of pressure is remarkable, considering that the elastic modulus of an elastomer is on the order of 1 MPa. Fracture mechanics has not been systematically applied to study the rupture of seals, although cracks are commonly observed in postmortem examinations. In practice, seals are tested in assembled parts, which are opaque and make the processes leading to leak unobservable.

Here we describe a method to study an elastomeric seal using its pressure-extrusion curves (i.e., the relation between the drop of pressure p and the volume of extrusion of the elastomer Q). We introduce a model sealing system that enables theoretical analysis and experimental observation. The theory calculates the finite elastic deformation of the seal and the energy release rate of the crack. The theoretical results are in analytical forms, and relate the pressure-extrusion curve to material and geometric parameters. We fabricate seals of various parameters in transparent chambers on a desktop, watch the seals extrude, slide, rupture and leak, and measure their pressure-extrusion curves. We then use independent experiments to determine elastic moduli, fracture energies, and sliding stresses (Appendix A, B, C), and use them to calculate the theoretical pressure-extrusion curves. The pressure-extrusion curves recorded in the experiment agree well with those calculated using the theory.

2. Modes of failure

The deformation of the elastomer is essential to both the function and failure of a seal. When the elastomer seals the fluid in a gap between stiff mating parts, the deformation of the elastomer enables it to adapt to unpredictable variations, such as the height of the gap, the misalignment of the mating parts, the roughness of their surfaces, and the change in temperature. Consequently, neither the seal nor the mating parts need be designed with high precision, which could be costly or impractical. However, the deformation of the elastomer may also lead to failure. The fluid pressure can cause the elastomer to extrude, which may lead to rupture, loss of contact, or even escape from the sealing site.

Incidentally, deformation of soft materials under constraint is also important in biology and medicine. For example, to measure the elastic properties of cells and other soft particles at the microscale, one can squeeze them through microfluidic channels (Guido and Tomaiuolo, 2009; Hou et al., 2009; Li et al., 2013; Li et al., 2015; She et al., 2012; Wyss et al., 2010).

The deformation of elastomers under constraint can be calculated by solving boundary-value problems. Due to the complexity of the problems, finite element methods are commonly adopted (George et al., 1987; Karaszkiewicz, 1990; Nikas, 2003). These calculations are challenging. The friction between the elastomer and mating parts is usually not well characterized in practice. The elastomers are nonlinear in their stress-strain behavior, and the conditions of rupture at sharp geometric features are not well understood. The boundary conditions are complex due to various sealing environments and contact conditions. Despite numerous efforts to calculate the deformation of seals, the relation between such calculations and the leaking pressure is still lacking.

On the basis of reports in the literature and our own preliminary experimental observations, we classify several modes of failure. Prior to the injection of fluid, an elastomeric seal is in a state of precompression between two rigid walls, and a step in the bottom wall defines the sealing site (Fig. 1a). As a pressurized fluid is injected into the space in front of the seal, the seal deforms, and extrudes at the other end at lower pressure. When the fluid pressure is high, a crack may initiate from the front of the seal and cross the length of the seal (Fig. 1b). Alternatively, a crack may form at the end of the seal and cut the extruded material (Fig. 1c). Both modes of damage have been widely observed (Flitney, 2007; Parker, 2007). Moreover, a seal may leak without any damage. Fluid can leak through the interface between the elastomer and the wall (Fig. 1d), a mode of failure which we call elastic leak (Liu et al., 2014; Wang et al., 2015). A seal can even squeeze into the tight space above the step, and escape from the sealing site (Fig. 1e). Each mode of failure requires a certain level of fluid pressure. The lowest one defines the sealing capability.

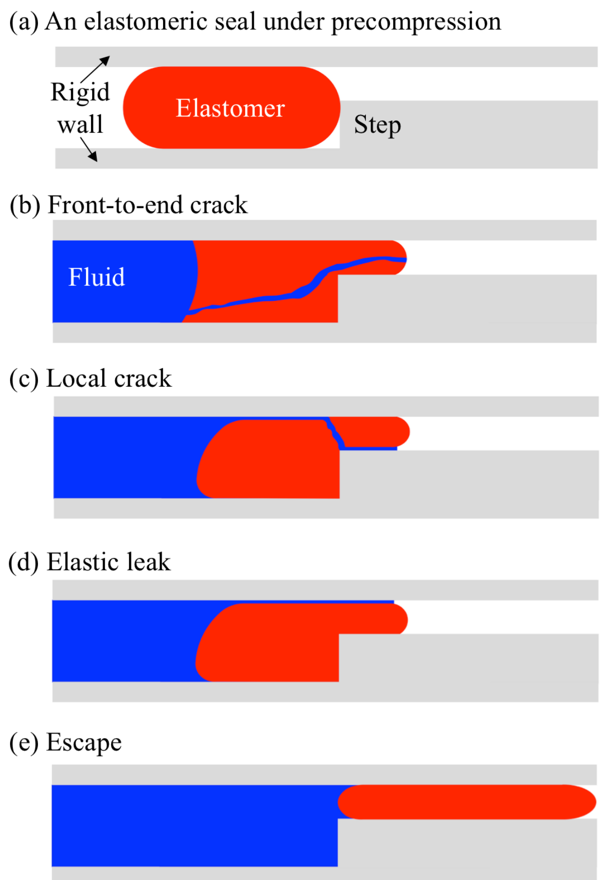

Fig. 1. Modes of failure of an elastomeric seal. (a) Prior to the injection of the fluid, a seal is in a state of precompression between two rigid walls, and a step in the bottom wall defines the sealing site. (b) A crack initiates from the front of the seal and propagates through the length of the seal. (c) A crack forms at the end of the seal and cuts the extruded elastomer. (d) Elastic leak without damage. Fluid penetrates into the interface between the elastomer and rigid wall. (e) Seal escapes from the sealing site.

To leak, or to rupture? This question deserves great attention. We have described elastic leak in previous papers (Liu et al., 2014; Wang et al., 2015). If a seal leaks before damage, one can lower the pressure to recover sealing. The elastic leak can serve as a design principle of a safety valve. Furthermore, elastic leak can improve sealing in certain designs, and can even be essential for the function of swellable seals. This paper will not discuss elastic leak any further, but will focus on the mode of failure caused by a crack across the length of the seal (Fig. 1b)

3. Extrusion and sliding

We now introduce a model sealing system. The model sealing system captures essential processes of a seal subject to a drop of pressure, such as extrusion of the elastomer, frictional sliding of the elastomer relative to a rigid wall, and the initiation and propagation of a crack. Consider a rectangular block of elastomer with the dimensions $L \times H \times B$ in the undeformed state (Fig. 2a). The elastomer is then placed between two rigid walls, in a state of precompression, with height h and length l (Fig. 2b). We assume that the precompression is homogeneous for simplicity. This assumption enables us to obtain an explicit analytical solution, which we will compare with experimental measurement. The elastomer is taken to be incompressible and deform under the plane strain conditions, so that $LH = lh$. The stretch $\lambda = h/H = L/l$ is a dimensionless measure of the precompression. After the precompression, the seal is bonded to the bottom wall, but not to the top wall. The bonding defines the sealing site, and no rigid step is introduced at the end of the seal. Because the elastomer is taken to be incompressible, its behavior is unaffected by any state of homogeneous hydrostatic pressure. The seal sustains a drop of pressure over its length. We apply this drop of pressure by injecting a fluid at the front of the seal at pressure p relative to the ambient pressure, and keeping the ambient pressure at the end of the seal. When the fluid pressure is low, the static friction between the seal and the top wall prevents seal from sliding (Fig. 2c). When the fluid pressure is high, the seal slides against friction (Fig. 2d).

Subject to the fluid pressure p, the seal deforms, and a volume Q of the elastomer crosses a vertical plane fixed in space. Because the elastomer is taken to be incompressible, Q is the same no matter where we fix the vertical plane. We call p the *fluid pressure* or the *drop* of *pressure*, Q the *volume of extrusion*, and the p-Q relation the *pressure-extrusion curve*. This curve characterizes the mechanical behavior of a seal, and can be readily measured in experiment. We have introduced the pressure-extrusion curve in our previous study of elastic leak (Liu et al., 2014). Here we highlight the importance of the pressure-extrusion curve in the study of sliding and rupture of a seal.

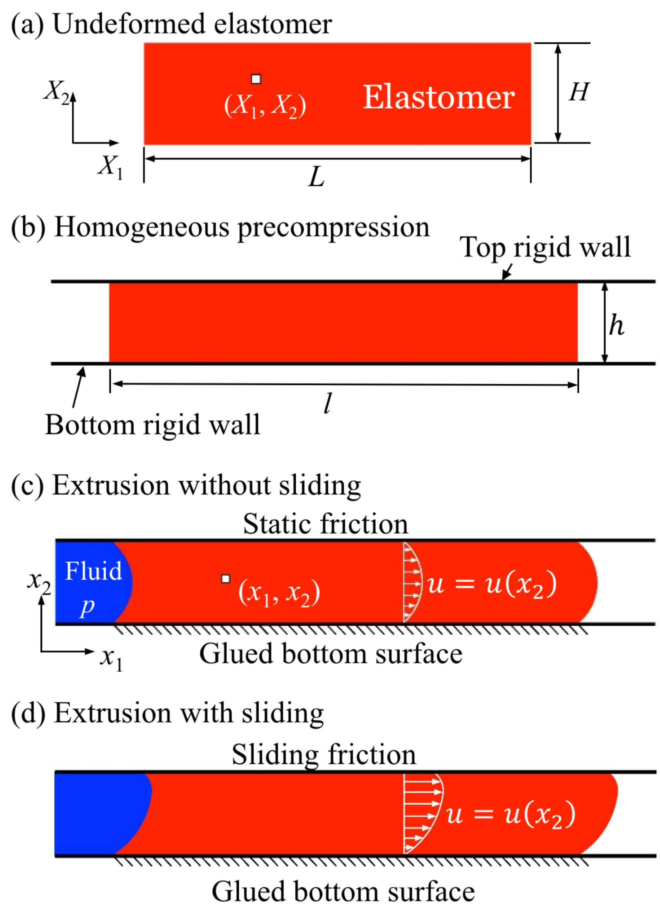

Fig. 2. The cross section of a seal under the plane strain conditions. (a) In the undeformed state, a material particle is specified by its coordinates (X_1, X_2). (b) The seal is uniformly pre-compressed by the rigid walls. (c) The seal is then bonded to the bottom wall, but not to the top wall. When a fluid pressure p is applied at the front of the seal, the seal deforms, and the material particle (X_1, X_2) moves to a place of coordinates (x_1, x_2). In the steady region, away from the two ends of the seal, the displacement profile is independent of x_1. When p is low, the elastomer does not slide relative to the top wall. (d) When p reaches to a critical value, the elastomer slides relative to the top wall.

Friction resists the sliding of the elastomer relative to the walls, and contributes to the sealing capacity of the seal. When the static friction prevents the elastomer from sliding, the displacement vanishes at the top surface of the elastomer. Our analytical solution predicts that the shear stress (i.e., the static frictional stress) acting on the top surface of the elastomer is everywhere the same along the length of the seal. When the elastomer slides relative to the top wall, the sliding stress depends on the model of kinetic friction. To simplify the analysis, we adopt an idealized model of kinetic friction: the elastomer bears a constant sliding stress τ. This constant-shear approximation has been commonly adopted in the shear-lag models of composites (e.g., (Hutchinson and Jensen, 1990)). We will compare the prediction of the theory based on this assumption to experiment. It is also known that friction between a hydrogel and a rigid wall is determined by the stretch and relaxation of polymer chains, and is less sensitive to the normal force (Gong et al., 1999; Liu et al., 2016). We will describe our own frictional sliding experiment to assess this assumption (Appendix C).

We develop a nonlinear elastic theory of the seal, and obtain an analytical solution of elastic deformation reminiscent of the Poiseuille flow in a viscous fluid. A material particle, labeled by the coordinates (X_1, X_2) in the undeformed state, moves to a place of coordinates (x_1, x_2) in the deformed state. Imagine that we mark a set of horizontal lines on the cross section of the seal in the state of precompression (Fig. 2b). Under the three assumptions—the plane strain conditions, incompressibility, and constant sliding stress—we expect that the fluid pressure will cause each horizontal line to translate horizontally, neither changing its length nor changing its height. Thus, we seek the deformation of the form

$$\begin{aligned} x_1 &= \lambda^{-1} X_1 + u(X_2), \\ x_2 &= \lambda X_2. \end{aligned} \quad (1)$$

The part $(x_1 = \lambda^{-1} X_1, x_2 = \lambda X_2)$ corresponds to a state of homogeneous precompression, and $u(X_2)$ is the horizontal displacement caused by the fluid pressure. We call the deformation (1) the *steady field*, and expect it to be valid in the seal away from the two ends, for the seal of a large aspect ratio, $L >> H$. As we will confirm, when the seal slides, the deformation (1) is consistent with the assumption of constant sliding stress.

Recall that a field of deformation $x_i(\mathbf{X})$ gives deformation gradient $F_{iK} = \partial x_i(\mathbf{X}) / \partial X_K$. Associated with the deformation (1), the deformation gradient is

$$\mathbf{F} = \begin{bmatrix} \lambda^{-1} & \lambda du(x_2)/dx_2 & 0 \\ 0 & \lambda & 0 \\ 0 & 0 & 1 \end{bmatrix}. \tag{2}$$

Note that we have changed the independent variable from X_2 to x_2, so that $du(X_2)/dX_2 = \lambda du(x_2)/dx_2$. As expected, the deformation gradient is independent of x_1. One can readily confirm that the deformation gradient is incompressible, $\det\mathbf{F} = 1$.

Let the in-plane components of the true stress be σ_{11}, σ_{22}, and σ_{12}, and the out-or-plane components be σ_{13}, σ_{23}, and σ_{33}. Under the plane strain conditions, components σ_{13} and σ_{23} vanish, while other components of the true stress in general vary with both x_1 and x_2. But the deformation (1) considerably simplifies the field of stress. For any incompressible elastic material, the material model requires that $\sigma_{11} - \sigma_{22}$, $\sigma_{33} - \sigma_{22}$ and σ_{12} be functions of the deformation gradient. Because the deformation gradient varies with x_2 but not with x_1, we write

$$\begin{aligned} &\sigma_{12} = \sigma_{12}(x_2), \\ &\sigma_{11} - \sigma_{22} = f(x_2), \\ &\sigma_{33} - \sigma_{22} = g(x_2). \end{aligned} \tag{3}$$

The functions $\sigma_{12}(x_2)$, $f(x_2)$, and $g(x_2)$ are to be determined by solving the boundary value problem.

Recall that the balance of forces requires that

$$\begin{aligned} &\frac{\partial \sigma_{11}}{\partial x_1} + \frac{\partial \sigma_{12}}{\partial x_2} = 0, \\ &\frac{\partial \sigma_{12}}{\partial x_1} + \frac{\partial \sigma_{22}}{\partial x_2} = 0. \end{aligned} \tag{4}$$

Equations (3) and (4) together require the field of stress take the following form:

$$\begin{aligned}
&\sigma_{12} = ax_2 + b,\\
&\sigma_{11} = -ax_1 + c + f(x_2),\\
&\sigma_{22} = -ax_1 + c,\\
&\sigma_{33} = -ax_1 + c + g(x_2).
\end{aligned} \tag{5}$$

The constants of integration, *a*, *b*, and *c*, are to be determined by the boundary conditions. Like the Poiseuille flow, the shear stress σ_{12} is linear in x_2 and is independent of x_1. Also like the Poiseuille flow, the normal stresses are linear in x_1, and σ_{22} is independent of x_2. Unlike the Poiseuille flow, however, σ_{11} and σ_{33} vary with both x_1 and x_2. Because of this dependence on x_2, the field of $\sigma_{11}(x_1, x_2)$ cannot satisfy the boundary conditions at the two ends of the seal point by point. Instead, we balance the resultant forces.

To determine *a*, use the entire seal as a free-body diagram. On the left side of the seal, the fluid pressure exerts a horizontal force hp. On the right side of the seal, the pressure is set to be zero, and no horizontal force is exerted on the seal. On the top surface of the seal, the shear stress exerts a horizontal force $l\sigma_{12}(h)$. Equation (5) relates the shear stress on the bottom of the seal to that on the top surface of the seal, $\sigma_{12}(0) = -ah + \sigma_{12}(h)$. Thus, on the bottom surface of the seal, the shear stress exerts a horizontal force $l(ah - \sigma_{12}(h))$. The balance of the forces acting on the seal in the horizontal direction gives that

$$a = -\lambda p / L. \tag{6}$$

To determine *c*, cut the seal vertically at any position x_1, and use the part on the right side as a free-body diagram. Equation (5) gives that $\sigma_{11} = -ax_1 + c + f(x_2)$, resulting in a horizontal force $ax_1 h - ch - \int_0^h f(x_2)dx_2$. The shear stress on the top surface exerts a horizontal force $(l - x_1 + u(h))\sigma_{12}(h)$. The shear stress on the bottom surface exerts a horizontal force

$-(l-x_1)\sigma_{12}(0)$, where we have assumed that the bottom surface does not slide, $u(0)=0$. There is no force acting on the right end of the seal. The balance of the forces acting on the seal in the horizontal direction gives that

$$c=\frac{1}{h}\left(\sigma_{12}(h)u(h)-\int_0^h f(x_2)dx_2\right)-p. \tag{7}$$

We write the field of stress in the seal as

$$\begin{aligned}
\sigma_{12} &= -\frac{\lambda p}{L}(x_2-\lambda H)+\sigma_{12}(h),\\
\sigma_{11} &= p\left(\frac{\lambda x_1}{L}-1\right)+\frac{1}{h}\left(\sigma_{12}(h)u(h)-\int_0^h f(x_2)dx_2\right)+f(x_2),\\
\sigma_{22} &= p\left(\frac{\lambda x_1}{L}-1\right)+\frac{1}{h}\left(\sigma_{12}(h)u(h)-\int_0^h f(x_2)dx_2\right),\\
\sigma_{33} &= p\left(\frac{\lambda x_1}{L}-1\right)+\frac{1}{h}\left(\sigma_{12}(h)u(h)-\int_0^h f(x_2)dx_2\right)+g(x_2).
\end{aligned} \tag{8}$$

This distribution is applicable to any incompressible elastic material.

We consider a neo-Hookean material characterized by the energy density function

$$W(\mathbf{F})=\frac{\mu}{2}(F_{iK}F_{iK}-3), \tag{9}$$

where μ is the shear modulus. Recall that, for an incompressible and elastic material, the true stress relates to the deformation gradient by

$$\sigma_{ij}=\frac{\partial W}{\partial F_{iK}}F_{jK}-\Pi\delta_{ij}, \tag{10}$$

where Π is the Lagrange multiplier to enforce incompressibility. Consequently, (3) specializes to

$$\sigma_{12}(x_2) = \mu\lambda^2 \frac{du(x_2)}{dx_2},$$
$$\sigma_{11} - \sigma_{22} = \mu\left[\left(\lambda \frac{du(x_2)}{dx_2}\right)^2 + \frac{1}{\lambda^2} - \lambda^2\right], \tag{11}$$
$$\sigma_{33} - \sigma_{22} = \mu(1-\lambda^2).$$

The seal is taken to be bonded to the bottom wall, $u(0)=0$. A comparison of the two expressions for the shear stress in (8) and (11) gives the field of displacement:

$$u(x_2) = \frac{p}{\mu L}\left(Hx_2 - \frac{x_2^2}{2\lambda}\right) + \frac{\sigma_{12}(h)}{\mu\lambda^2} x_2 \ . \tag{12}$$

The displacement in the seal is independent of x_1, and is parabolic in x_2. This field of displacement in the elastic seal is analogous to that of velocity in the Poiseuille flow.

The field of stress can be obtained by substituting (12) and (2) into (10):

$$\sigma_{12} = p\left(\frac{\lambda^2 H}{L} - \frac{\lambda x_2}{L}\right) + \sigma_{12}(h),$$
$$\sigma_{11} = p\left(\frac{\lambda x_1}{L} + \frac{\sigma_{12}(h)H}{2\mu L} - 1\right) + \frac{p^2}{\mu}\left[\left(\frac{x_2 - \lambda H}{L}\right)^2 - \frac{1}{3}\left(\frac{\lambda H}{L}\right)^2\right] + \frac{\sigma_{12}^2(h)}{\mu\lambda^2},$$
$$\sigma_{22} = p\left(\frac{\lambda x_1}{L} + \frac{\sigma_{12}(h)H}{2\mu L} - 1\right) - \frac{1}{3\mu}\left(\frac{\lambda p H}{L}\right)^2 - \mu\left(\frac{1}{\lambda^2} - \lambda^2\right) + \frac{\sigma_{12}^2(h)}{\mu\lambda^2}, \tag{13}$$
$$\sigma_{33} = p\left(\frac{\lambda x_1}{L} + \frac{\sigma_{12}(h)H}{2\mu L} - 1\right) - \frac{1}{3\mu}\left(\frac{\lambda p H}{L}\right)^2 - \mu\left(\frac{1}{\lambda^2} - 1\right) + \frac{\sigma_{12}^2(h)}{\mu\lambda^2}.$$

The stresses are nonlinear in precompression, indicating that the linear elastic assumption used in many soft particle studies (Li et al., 2013; Wyss et al., 2010) is only valid when compression is small. σ_{11} , σ_{22} and σ_{33} drop linearly along x_1, but σ_{12} is independent of x_1, confirming the assumption of constant shear stress along x_1. σ_{22} and σ_{33} are independent of x_2, σ_{12} is linear in x_2, and σ_{11} is parabolic in x_2. Stresses concentrate at the front corner at the bottom.

In the non-sliding stage (Fig. 2c), the displacement of the upper surface of the seal vanishes, $u(h)=0$, and (12) determines the static frictional stress $\sigma_{12}(h)=-pH\lambda^2/(2L)$. We require that the static frictional stress be below the sliding stress, $pH\lambda^2/(2L)<\tau$. In the sliding stage (Fig. 2d), our assumption dictates that the shear stress be the constant sliding stress, $\sigma_{12}(h)=-\tau$. The transition between these two stages occurs at the pressure $p=2L\tau/(H\lambda^2)$.

We look into the stress state of the bottom corner where stresses concentrate most. The normal stresses are always compressive, which does not allow mode I fracture. As will be described in the next section, our experiment shows that the crack initiates at the front-bottom of the seal, but propagates into the gel.

We rewrite (12) as

$$u(x_2)=\begin{cases} \dfrac{p}{\mu L}\left(\dfrac{Hx_2}{2}-\dfrac{x_2^2}{2\lambda}\right), & \text{when } p<\dfrac{2L\tau}{H\lambda^2}, \\ \dfrac{p}{\mu L}\left(Hx_2-\dfrac{x_2^2}{2\lambda}\right)-\dfrac{\tau}{\mu\lambda^2}x_2, & \text{when } p\geq\dfrac{2L\tau}{H\lambda^2}. \end{cases} \tag{14}$$

The integration of the displacement profile gives the volume of extrusion:

$$Q=B\int_0^h u\,dx_2 \,. \tag{15}$$

The pressure-extrusion relation takes the form:

$$p=\begin{cases} 12\dfrac{\mu QL}{BH^3\lambda^2}, & \text{when } p<\dfrac{2L\tau}{H\lambda^2}, \\ 3\dfrac{\mu QL}{BH^3\lambda^2}+\dfrac{3}{2}\dfrac{L\tau}{H\lambda^2}, & \text{when } p\geq\dfrac{2L\tau}{H\lambda^2}. \end{cases} \tag{16}$$

The pressure-extrusion relation is bilinear, with a change in slope when the seal starts to slide relative to the top wall (Fig. 3). The intercept of the line for the sliding stage is given by $p=(3L\tau)/(2H\lambda^2)$. The shear modulus μ affects the slopes of both lines, and the sliding stress τ affects the intercept of the line for the sliding stage.

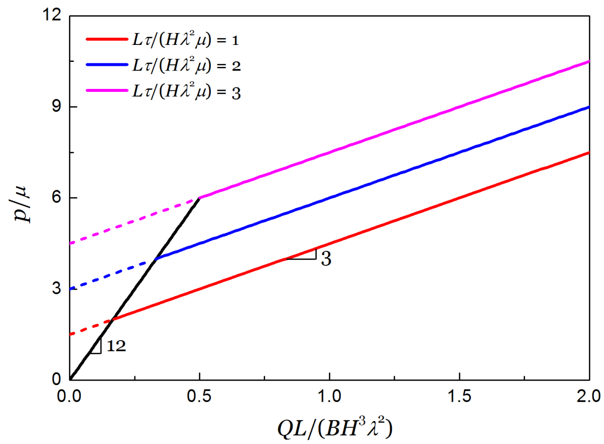

Fig. 3. Theoretical relation between the fluid pressure p and the volume of extrusion Q, plotted in a dimensionless form. The non-sliding stage corresponds to a straight line with slope 12. The sliding stage corresponds to a straight line with slope 3, and the level depends on the normalized sliding stress $L\tau/\left(H\lambda^2\mu\right)$.

4. Rupture

This section applies fracture mechanics to the mode of failure due to a crack that runs across the length of a seal (Fig. 1b). The critical pressure for the onset of the propagation will depend on the initial crack. This section will analyze an idealized model, and the next section will compare the model to the experiment.

Our model assumes an initial debonded part of length l_c, located at the front-bottom of the seal (Fig. 4). The model further assumes that both the top surface of the seal and the debonded part bear the same sliding stress τ. The model calculates the energy release rate for the extension of the debond. Except for small regions near the tip of the debond and the two ends of the seal, the displacement fields in the debonded and bonded regions are independent of x_1, and are denoted as $u_c(x_2)$ and $u_b(x_2)$, respectively. These two steady fields can be obtained using the work in the previous section.

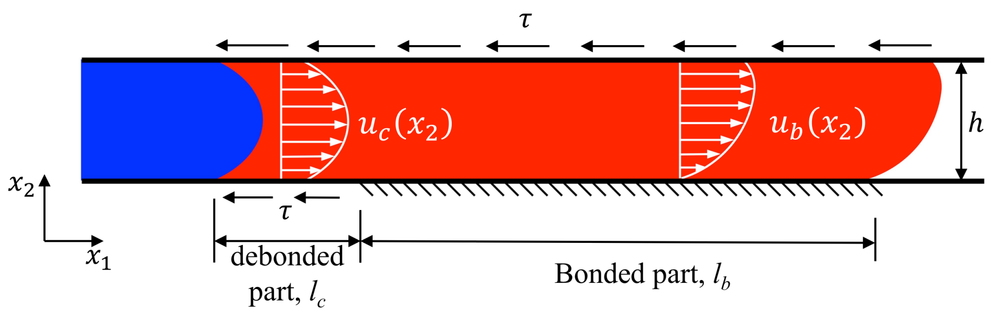

Fig. 4. An idealized model of rupture. The model assumes a debonded part of length l_c located at the front-bottom of the seal. The debonded part of the seal slides against the bottom wall with a constant frictional stress, which we assume identical to the frictional stress at the top interface τ. Except for the regions near the tip of the debond and the two ends of the seal, the seal is modeled by two steady states, with displacement profiles $u_c(x_2)$ and $u_b(x_2)$.

The fluid pressure p drops over the entire length of the seal—that is, over the debonded and the bonded parts in series. The drop of pressure over the debonded part, p_c, is balanced by the sliding stress on the top and bottom surface of the seal, so that

$$p_c = \frac{2\tau L_c}{\lambda^2 H} . \tag{17}$$

Here L_c is the length of the crack when the seal is in the undeformed state, $L_c = \lambda l_c$. The drop of pressure over the bonded part, p_b, is given by $p_b = p - p_c$, namely,

$$p_b = p - \frac{2\tau L_c}{\lambda^2 H} . \tag{18}$$

The displacement field in the debonded region is identical to that in the non-sliding stage, but with an additional rigid-body translation u_0 due to the extrusion of the elastomer (Fig. 2c). The displacement field in the bonded region is identical to that in the sliding stage (Fig. 2d). Therefore, $u_c(x_2)$ and $u_b(x_2)$ can be obtained by substituting (17) and (18) into (12):

$$\begin{aligned} u_c(x_2) &= u_0 - \frac{\tau}{H\mu\lambda^3}\left(x_2 - \frac{\lambda H}{2}\right)^2, \\ u_b(x_2) &= \frac{p - \left(2\tau L_c / \lambda^2 H\right)}{2\mu L_c}\left(2Hx_2 - \frac{x_2^2}{\lambda}\right) - \frac{\tau}{\mu\lambda^2}x_2. \end{aligned} \tag{19}$$

The value of u_0 can be determined by the condition of incompressibility:

$$\int_0^h u_c(x_2)dx_2 = \int_0^h u_b(x_2)dx_2 . \tag{20}$$

Substituting (19) into (20) gives that

$$u_0 = \frac{pH^2\lambda}{3\mu L_b} - \left(\frac{5}{12} + \frac{2L_c}{3L_b}\right)\frac{\tau H}{\lambda\mu} . \tag{21}$$

The displacements at the sliding surfaces of the debonded region are

$$u_c(0) = u_c(h) = \frac{pH^2\lambda}{3\mu L_b} - \frac{2}{3}\left(1 + \frac{L_c}{L_b}\right)\frac{\tau H}{\lambda\mu} . \tag{22}$$

The displacement at the sliding surface of the bonded region is

$$u_b(h) = \frac{p\lambda H^2}{2\mu L_b} - \frac{\tau H}{\mu\lambda}\left(1 + \frac{L_c}{L_b}\right). \tag{23}$$

The volume of extrusion Q is given by $Q = B\int_0^h u_c(x_2)dx_2 = B\int_0^h u_b(x_2)dx_2$. A direct calculation gives that

$$Q = \frac{pH^3B}{3\mu L_b}\lambda^2 - \left(\frac{1}{2} + \frac{2L_c}{3L_b}\right)\frac{\tau H^2 B}{\mu}. \tag{24}$$

We next calculate the energy release rate of the crack. The deformation gradients in the debonded and bonded regions, $\mathbf{F}_c$ and $\mathbf{F}_b$, are functions of x_2. The elastic energy in the debonded region is $U_c = Bl_c\int_0^h W(\mathbf{F}_c)dx_2$, giving

$$U_c = \frac{\tau^2 L_c HB}{6\mu\lambda^2} + \frac{\mu}{2}\left(\lambda^2 + \lambda^{-2} - 2\right)BHL_c . \tag{25}$$

The elastic energy in the bonded region is $U_b = Bl_b\int_0^h W(\mathbf{F}_b)dx_2$, giving

$$U_b = \frac{p^2H^3B}{6\mu L_b}\lambda^2 - \frac{p\tau H^2 B}{\mu}\left(\frac{2L_c}{3L_b} + \frac{1}{2}\right) + \frac{\tau^2 HB}{\mu\lambda^2}\left(\frac{2L_c^2}{3L_b} + \frac{L_b}{2} + L_c\right) + \frac{\mu}{2}\left(\lambda^2 + \lambda^{-2} - 2\right)BHL_b. \tag{26}$$

The potential energy of the seal is a function $\Phi\left(p,\tau,L_c\right)$, including the elastic energy in the seal and the potential energy of all fixed loads:

$$\Phi\left(p,\tau,L_c\right)=U_c+U_b-pQ+2Bl_c\tau u_c\left(0\right)+Bl_b\tau u_b\left(h\right). \tag{27}$$

Here we regard the fluid pressure p and the sliding stress τ as fixed loads. The above calculation gives that

$$\Phi\left(p,\tau,L_c\right)=-\frac{p^2H^3\lambda^2B}{6\mu L_b}-\frac{\tau^2HL_bB}{\mu\lambda^2}\left(\frac{1}{2}+\frac{7}{6}\frac{L_c}{L_b}+\frac{2}{3}\left(\frac{L_c}{L_b}\right)^2\right)+\frac{p\tau H^2B}{\mu}\left(\frac{1}{2}+\frac{2L_c}{3L_b}\right). \tag{28}$$

Recall that the energy release rate is defined as the reduction of the potential energy associated with the crack advancing per unit area:

$$G=-\frac{\partial\Phi\left(p,\tau,L_c\right)}{B\partial L_c}. \tag{29}$$

A direct calculation gives the energy release rate:

$$G=\frac{H}{6\mu L_b^2}\left(pH\lambda-\frac{2\tau L}{\lambda}\right)^2. \tag{30}$$

The energy release rate increases with the fluid pressure p and decreases with the sliding stress τ. In the non-sliding stage, $pH\lambda<2\tau L\lambda^{-1}$, the energy release rate is zero and the crack remains stationary regardless of the crack size and the fluid pressure. This result is consistent with the assumption that crack propagates after the seal slides. In addition, the energy release rate increases with the crack length L_c (equivalent to the decrease of L_b). We assume that the length of the initial crack is small compared to the total length of the seal, $L_c<<L$. Setting $L_c=0$, we obtain that

$$G=\frac{H}{6\mu L^2}\left(pH\lambda-\frac{2\tau L}{\lambda}\right)^2. \tag{31}$$

We will use this expression to compare with experimental measurements.

When the energy release rate G reaches the fracture energy Γ, the initial crack propagates. Inserting (31) into $G = \Gamma$, we obtain the critical fluid pressure for the onset of the propagation of the crack:

$$p_f = \frac{\sqrt{6}}{\lambda}\sqrt{\frac{\Gamma\mu}{H}}\frac{L}{H} + \frac{2\tau L}{H\lambda^2}. \qquad (32)$$

This critical pressure defines the sealing capacity of a seal. The above equation relates the critical fluid pressure to six parameters. The sealing capability can be increased by choosing stiffer and tougher material, by extending the length and reducing the thickness, by increasing the sliding stress, and by increasing precompression. Everything else being fixed, the critical fluid pressure is linear in the length of the seal.

5. Experimental measurement and discussion

We set up a transparent device to watch seals extrude, slide, rupture, and leak *in situ* (Supplementary Movies 1 and 2). We use a block of hydrogel as the sealing element. The hydrogel has much lower values of elastic modulus, sliding stress, and fracture energy, compared to those of elastomers used in the oil and gas industry. This is so that we can perform the experiments at low fluid pressure on a desktop. The object of the experiment is to assess the assumptions of the idealized theoretical model. To study the effect of material parameters on the leaking pressure, we synthesize polyacrylamide hydrogels with different water contents and crosslink densities, and measure the shear moduli, fracture energies, and sliding stresses (Table 1, Appendix A-C). We do not attempt to vary the shear modulus, fracture energy, and sliding stress independently.

In the setup for the sealing test, a block of the hydrogel, of the dimensions L, B and H in the undeformed state, is glued to a transparent acrylic sheet and spacer (Fig. 5a). The spacer has the same height H as the undeformed hydrogel. The acrylic sheet is glued to a base glass sheet. Another acrylic sheet of thickness ΔH and width B is glued to the cover glass sheet. When the cover glass sheet is glued on the top of the spacer, the hydrogel is compressed with a stretch

$\lambda = (H - \Delta H)/H$ (Fig. 5b). No adhesive is applied between the cover acrylic sheet and hydrogel. The base and cover glass sheets serve as the rigid walls to confine the hydrogel, while keeping the device transparent. The acrylic sheets, spacer, and hydrogel form a chamber, which connects to a syringe pump and a pressure gauge by plastic tubes via two drilled holes on the two sides of the spacer. The syringe pump injects water into the chamber at a constant rate 2ml/min. The volume of injected fluid, denoted as Q_i, is recorded as a function of the fluid pressure p. A digital camera monitors the movement of the hydrogel (colored red) and water (colored blue).

Table 1. Composition of polyacrylamide hydrogels and measured shear modulus, fracture energy, and sliding stress.

Material designation	Water (wt%)	MBAA/AAM (wt%)	Shear modulus, μ (kPa)					Fracture energy, Γ (J/m^2)					Sliding stress, τ (kPa)			
			1	2	3	Mean	STD	1	2	3	Mean	STD	1	2	Mean	STD
M-92-06	92.00	0.60	2.20	1.79	1.75	1.91	0.25	13.57	10.89	13.76	12.74	1.61	3.00	3.18	3.09	0.13
M-92-12	92.00	1.20	3.23	2.99	2.76	2.99	0.24	8.85	6.78	6.44	7.36	1.30	3.47	3.70	3.58	0.16
M-92-24	92.00	2.40	3.96	3.84	4.04	3.95	0.10	4.18	3.52	4.60	4.10	0.55	3.85	4.45	4.15	0.42
M-88-06	88.00	0.60	7.06	6.40	6.53	6.66	0.35	13.88	11.98	11.61	12.49	1.21	7.54	7.53	7.54	0.01

Ideally, the volume of injected fluid Q_i is identical to the volume of extrusion Q of the elastomer. However, the syringe pump and plastic tubes expand under pressure. To calibrate this effect, we directly connect the plastic tubes of the syringe pump and pressure gauge, and record the volume of injected fluid, Q_s, as a function of p (Fig. 5c). We then calibrate the volume of extrusion as $Q = Q_i - Q_s$ (Fig. 5d).

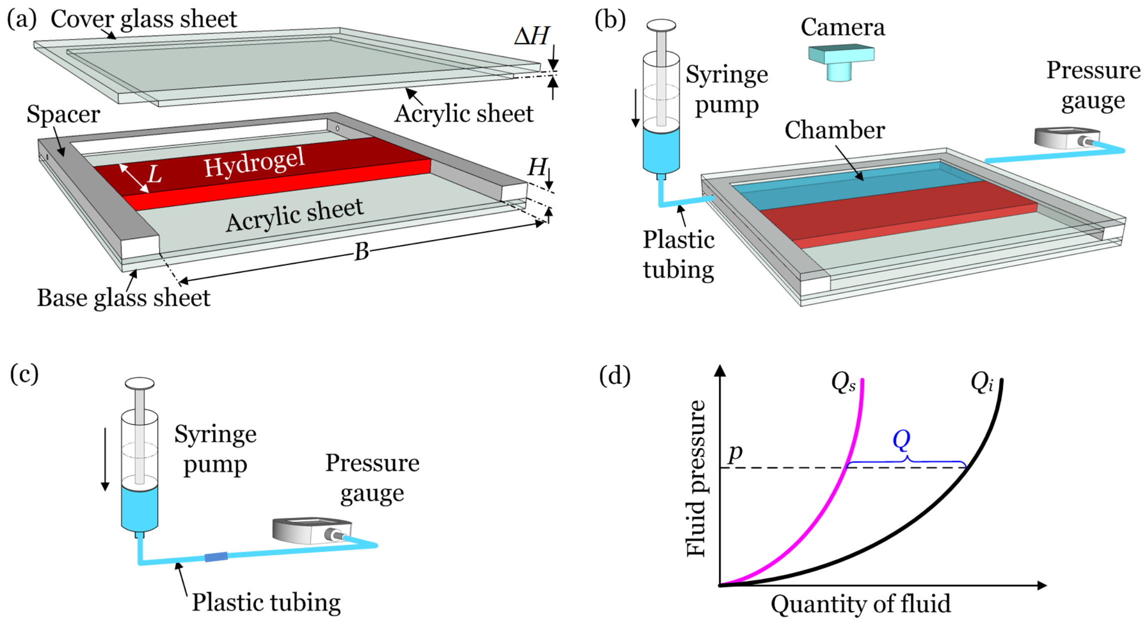

Fig. 5. Schematics of the sealing test. (a) A block of hydrogel, of dimensions H, L and B in the undeformed state, is glued to an acrylic sheet and a spacer with same height H. The acrylic sheet is attached to a sheet of glass (base glass sheet). An acrylic sheet of thickness ΔH is attached to another sheet of glass (cover glass sheet). (b) When the cover sheet is glued to the spacer, the hydrogel is precompressed with a displacement ΔH. The acrylic sheets, spacer and hydrogel form a chamber, which connects to a syringe pump and a pressure gauge. As the syringe pump injects fluid at a constant rate into the chamber, the pressure gauge measures the fluid pressure in the chamber, p. (c) Conntect the plastic tubes directly, and measure the volume of injected fluid, Q_s, as a function of p. (d) Measure the total volume of injected fluid Q_i and determine the volume of extrusion as $Q = Q_i - Q_s$ for a given p.

Figure 6 shows the results of a representative experiment. The volumes of injected fluid with or without sealing elements, Q_i and Q_s, are measured as functions of pressure (Fig. 6a). Note that Q_s is indeed non-negligible compared with Q_i. At any given fluid pressure p, we determine the volume of extrusion by $Q = Q_i - Q_s$, and then plot the p-Q relation. The normalized p-Q relation is nearly bilinear and a change in slope is evident (Fig. 6b).

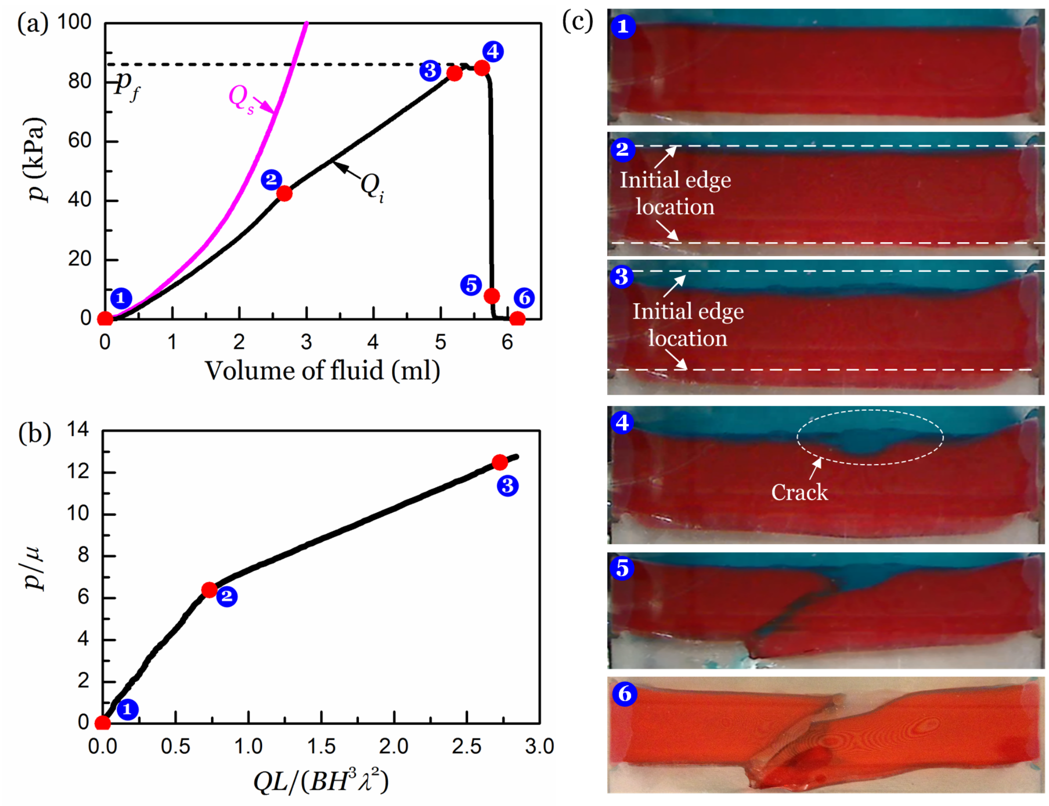

Fig. 6. Results of a sealing test. A hydrogel (M-88-06), of dimensions H = 6.00 mm, L = 20.00 mm, and B = 120.00 mm, is compressed with a stretch of $\lambda = 0.83$. The syringe pump injects water at a constant rate of 2ml/min until the seal leaks. (a) The fluid pressure, p, is recorded as functions of the volume of injection, with or without the seal, Q_i and Q_s. (b) The normalized relation between the fluid pressure, p, and the volume of extrusion, Q. (c) Six snapshots of the seal in the states marked in (a).

The transparent setup enables us to watch a seal extrude, slide, and rupture, while the fluid pressure is increased (Fig. 6c). Snapshot 1 shows the precompressed seal without the fluid pressure. When the fluid pressure is low, the hydrogel does not slide against the top wall and the deformation of the seal is small (snapshot 2). As the fluid pressure increases beyond a certain value, The hydrogel slides against the top wall (snapshot 3). When the fluid pressure reaches its maximum, p_f, a crack initiates at the front-bottom of the seal and propagates parallel and close to the bottom wall (snapshot 4). Subsequently, the crack turns into a centered crack perpendicular to the bottom wall and propagates through the length of the seal (snapshot 5). After the seal ruptures, water leaks through the crack. Snapshot 6 shows the residual deformation after the fluid is removed. A thin layer of hydrogel remains on the acrylic sheet in the bottom. This observation indicates that the crack initiates and propagates in the hydrogel rather than along the interface between the hydrogel and the acrylic.

Thus, the process of rupture may be divided into two stages: initiation and propagation of a crack. At the first stage, the crack just initiates in the gel, at the front-bottom of the seal, and the crack path is almost the same as that in the analytical model. At the second stage, the crack becomes perpendicular to the rigid walls, and is different from that in the model.

The initiation of the crack corresponds to the peak of the recorded pressure-extrusion curve (Fig. 6a). The model in Section 4 is used to calculate the energy release rate for the growth of the crack in this initial stage. The fracture energy of the bulk hydrogel, rather than that of the hydrogel/acrylic interface, is used in the rupture criterion. The model gives a prediction of the critical pressure (32). After the crack initiates in the gel, its subsequent propagation is unstable, corresponding to a rapid drop of pressure. The subsequent crack propagation is a complex process, but is beyond our goal to predict the critical pressure. In this paper we do not model the subsequent propagation of crack.

We conduct the experiment for sixteen seals of different values of material and geometric parameters (Table 2), and record the pressure-extrusion curves (Fig. 7). For each seal, the pressure-extrusion curve includes both the non-sliding stage and the sliding stage, and is terminated at the critical fluid pressure at the onset of crack propagation. The change in slope from non-sliding to sliding stages is sharp in some cases, but smooth in others. One possibility is that the sliding stress is nonuniform, and the contact surface does not slide simultaneously.

We next compare the results of the sealing test to our theory. Our theory identifies six parameters that affect sealing capacity: the shear modulus μ, fracture energy Γ, sliding stress τ, length L, thickness H, and precompression λ. As described above, we measure all the six parameters by experiments independent of the sealing test, and list their values in Tables 1 and 2. Our theory gives two principal results: the pressure-extrusion curve during the non-sliding and the sliding stages (16), and the critical fluid pressure at the onset of crack propagation (32). Included in Fig. 7 are the plots of equations (16) and (32) using the six parameters (Table 1 and 2) determined in the independent experiments (Appendix A, B, C). The agreement between the experiment and theory is remarkable.

Table 2. Experimentally measured leaking pressure for seals of different values of parameters.

Material	L (mm)	H (mm)	λ	p_f (kPa)
M-92-06	15.00	6.00	0.74	40.60
M-92-12	15.00	6.00	0.74	53.50
M-92-24	15.00	6.00	0.74	51.40
M-88-06	15.00	6.00	0.74	100.60
M-88-06	15.00	6.00	0.83	72.10
M-88-06	20.00	6.00	0.83	85.70
M-88-06	25.00	6.00	0.83	133.60
M-88-06	30.00	6.00	0.83	175.10
M-92-24	30.00	4.50	0.93	91.20
M-92-24	30.00	6.00	0.93	80.40
M-92-24	30.00	9.00	0.93	36.90
M-92-24	30.00	12.00	0.93	27.10
M-92-12	15.00	6.00	0.96	29.60
M-92-12	15.00	6.00	0.86	39.60
M-92-12	15.00	6.00	0.74	53.50
M-92-12	15.00	6.00	0.61	57.30

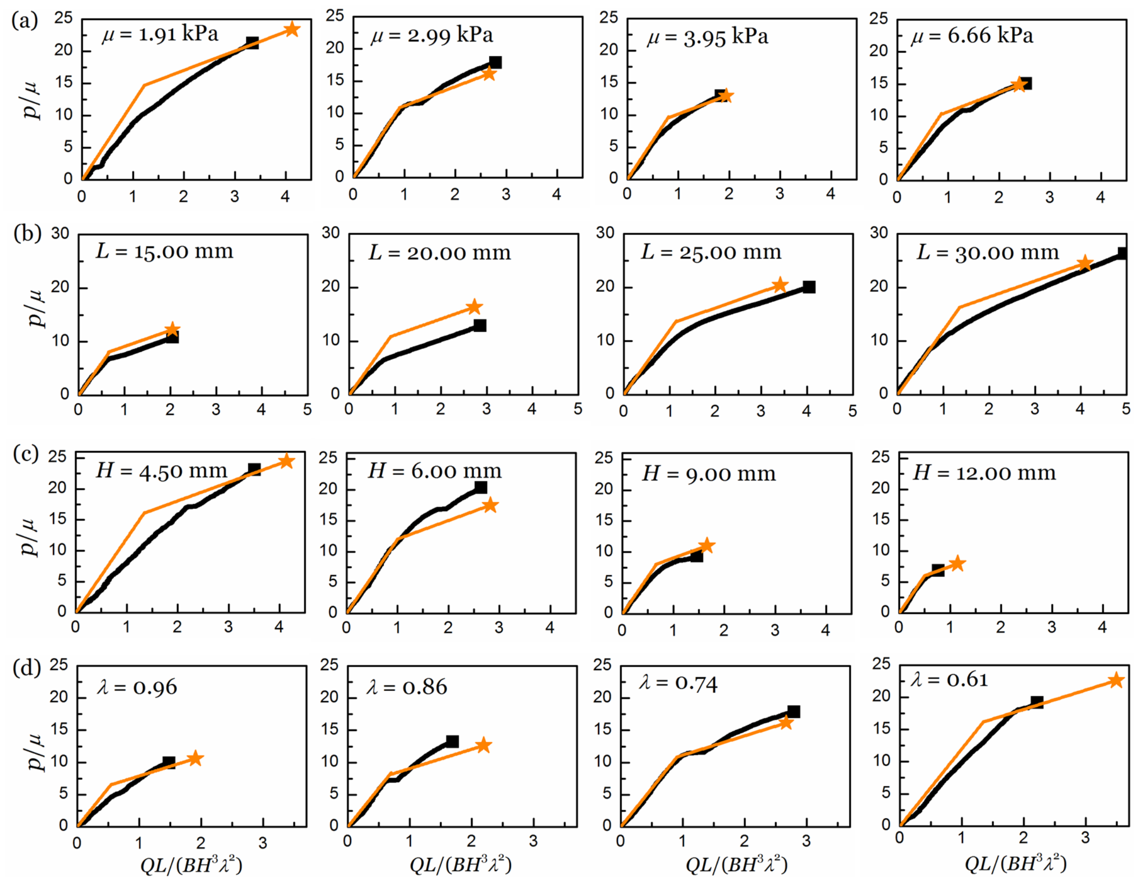

Fig. 7. The dimensionless pressure-extrusion curves for seals of different values of parameters. The black lines are experimental results. The orange lines are theoretical predictions. The sixteen seals correspond to those listed in Table 2.

Figure 8 plots the variation of the leaking pressure with respect to different geometrical variables. The leaking pressure increases with L, and decreases with H and λ. The experimentally measured leaking pressures agree well with the theoretical predictions. The latter are obtained by plotting (32) using the materials properties (fracture energy, elastic modulus, and sliding stress) measured in independent experiments (Table 1).

The critical fluid pressures measured in the sealing test also agree well with those predicted theoretically (Fig. 9). The theoretical predictions of the critical fluid pressure are calculated from equation (32) using the six parameters determined in the independent experiments (Tables 1 and 2, Appendices A-C).

Inspecting the two equations (16) and (32) again, we observe that elastic modulus μ, sliding stress τ, and fracture energy Γ correspond to three distinct features of the pressure-extrusion relation. The elastic modulus μ affects the two slopes of the bilinear relation, the sliding stress τ sets the intercept of the sliding part of the relation, and the fracture energy Γ appears in the expression for the critical fluid pressure. The good agreement between the theory and experiment, of course, suggests that the pressure-extrusion curve of a seal may be used to measure the shear modulus, sliding stress, and fracture energy *in-situ*.

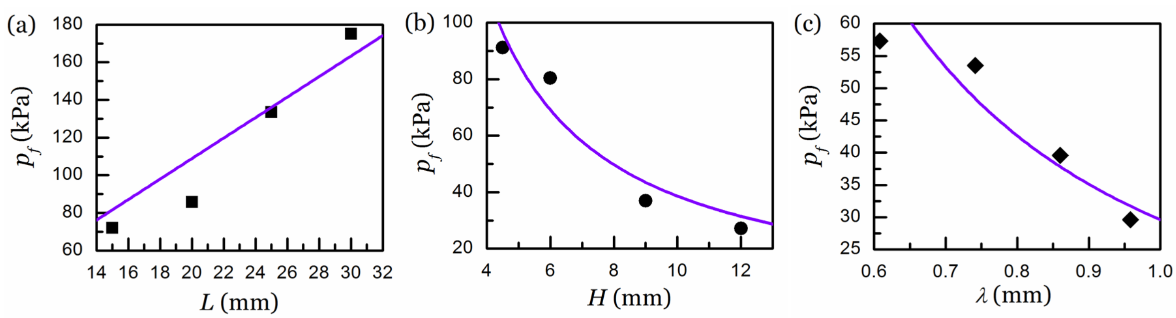

Fig. 8. Relations between the leaking pressure p_f and different geometrical parameters. The dots are experimental results, and the curves are theoretical predictions. (a) $\mu = 6.66$ kPa (M-88-06), H = 6.00 mm, $\lambda = 0.83$, L varies from 15.00 mm to 30.00 mm. (b) $\mu = 3.95$ kPa (M-92-24), L = 30.00 mm, $\lambda = 0.93$, H varies from 4.50 mm to 12.00 mm. (c) $\mu = 2.99$ kPa (M-92-12), L = 15.00 mm, H = 6.00 mm, λ varies from 0.96 to 0.61.

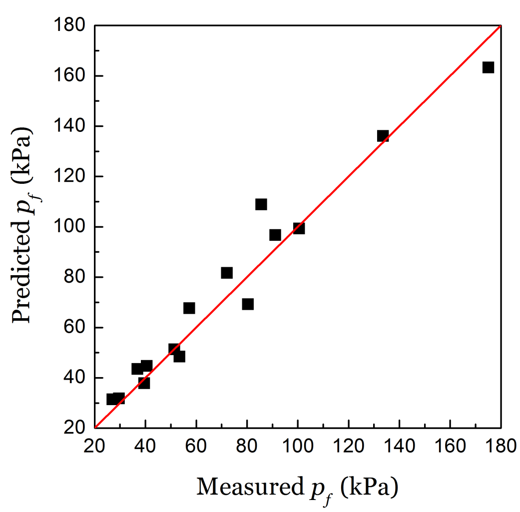

Fig. 9. Comparison between experimental results and theoretical predictions of the leaking pressure p_f.

6. Conclusion

We show that the pressure-extrusion curve is an effective tool to study the behavior of a seal. We introduce an idealized model that enables theoretical analysis and experimental observation. The theory calculates the pressure-extrusion curves for various material and geometric parameters. We fabricate seals of different values of the parameters, install them in transparent chambers on a desktop, and watch them extrude, slide, rupture, and leak. The experimental measured and theoretical predicted pressure-extrusion curves are in good agreement. The principal factors—elastic modulus, sliding stress, and fracture energy—correspond to distinct features on the pressure-extrusion curve. The good agreement between the theory and experiment suggests that the pressure-extrusion curve provides a method for the *in situ* measurement of elastic modulus, sliding stress, and fracture energy of soft materials under constraints. We hope that this work will guide the future development and field test of elastomeric seals.

Acknowledgement

Work at Harvard is supported by MRSEC (DMR-0820484) and by Schlumberger. Wang is supported by China Scholarship Council as a visiting scholar for two years at Harvard University. We thank Professors David Mooney and Joost Vlassak for the use of their laboratories.

References

Al Douseri, K.M., Barnes, C.G., Young, D.A., Smith, P.E., 2009. Swellable Packers Provide a Brownfield Water Management Solution in Open and Cased Hole – Case Histories Including Straddles, Plugs, Slimhole Sidetracks and Testing In Corroded Casing, Offshore Europe. Society of Petroleum Engineers, Aberdeen, UK.

Cai, S., Lou, Y., Ganguly, P., Robisson, A., Suo, Z., 2010. Force generated by a swelling elastomer subject to constraint. Journal of Applied Physics 107, 103535.

Coronado, M.P., Bjørkesett, H., Jiral, D.G., Førdedal, H., 2002. Advanced Openhole Completions Utilizing a Simplified Zone Isolation System, SPE Annual Technical Conference and Exhibition. Society of Petroleum Engineers, San Antonio, Texas, USA.
Davis, T.W., McCrady, D.D., 2008. Using Swellable Packers To Provide Annular Isolation for Multistage Fracture Treatments, SPE Annual Technical Conference and Exhibition. Society of Petroleum Engineers, Denver, Colorado, USA.
Druecke, B., Dussan V., E.B., Wicks, N., Hosoi, A.E., 2015. Large elastic deformation as a mechanism for soft seal leakage. Journal of Applied Physics 117, 104511.
Ezeukwu, T., Awi, H., Martinson, T., Stenger, B., Guinot, F., 2007. Successful Installation of Elastomeric Packers/Expandable Sand Screen in Subsea Openhole Completions Offshore Nigeria, Nigeria Annual International Conference and Exhibition. Society of Petroleum Engineers, Abuja, Nigeria.
Flitney, R., 2007. Seals and Sealing Handbook, Fifth Edition ed. Elsevier Science, Oxford.
Gavioli, P., Vicario, R., 2012. The Evolution of the Role of Openhole Packers in Advanced Horizontal Completions: From Novel Technology to a Critical Key to Success. SPE-117709-PA 27, 75 - 93.
Gent, A.N., 2012. Engineering with Rubber(Third Edition). Hanser.
George, A.F., Strozzi, A., Rich, J.I., 1987. Stress fields in a compressed unconstrained elastomeric O-ring seal and a comparison of computer predictions and experimental results. Tribology International 20, 237-247.
Gong, J., Iwasaki, Y., Osada, Y., Kurihara, K., Hamai, Y., 1999. Friction of Gels. 3. Friction on Solid Surfaces. The Journal of Physical Chemistry B 103, 6001-6006.
Guido, S., Tomaiuolo, G., 2009. Microconfined flow behavior of red blood cells in vitro. Comptes Rendus Physique 10, 751-763.
Hou, H.W., Li, Q.S., Lee, G.Y.H., Kumar, A.P., Ong, C.N., Lim, C.T., 2009. Deformability study of breast cancer cells using microfluidics. Biomedical Microdevices 11, 557-564.
Hutchinson, J.W., Jensen, H.M., 1990. Models of fiber debonding and pullout in brittle composites with friction. Mechanics of Materials 9, 139-163.
Karaszkiewicz, A., 1990. Geometry and contact pressure of an O-ring mounted in a seal groove. Industrial & Engineering Chemistry Research 29, 2134-2137.
Kleverlaan, M., van Noort, R.H., Jones, I., 2005. Deployment of Swelling Elastomer Packers. Journal of petroleum technology 57, 45-46.
Li, Y., Kumacheva, E., Ramachandran, A., 2013. The motion of a microgel in an axisymmetric constriction with a tapered entrance. Soft Matter 9, 10391-10403.
Li, Y., Sarıyer, O.S., Ramachandran, A., Panyukov, S., Rubinstein, M., Kumacheva, E., 2015. Universal behavior of hydrogels confined to narrow capillaries. Scientific Reports 5, 17017.
Liu, Q., Wang, Z., Lou, Y., Suo, Z., 2014. Elastic leak of a seal. Extreme Mechanics Letters 1, 54-61.
Liu, T., Jagota, A., Hui, C.-Y., 2016. Effect of surface tension on the adhesion between a rigid flat punch and a semi-infinite neo-Hookean half-space. Extreme Mechanics Letters 9, Part 2, 310-316.
Lou, Y., Chester, S., 2014. Kinetics of Swellable Packers under Downhole Conditions. International Journal of Applied Mechanics 06, 1450073.
Miller, J.T., Su, T., Pabon, J., Wicks, N., Bertoldi, K., Reis, P.M., 2015. Buckling of a thin elastic rod inside a horizontal cylindrical constraint. Extreme Mechanics Letters 3, 36-44.

Nau, B.S., 1999. An historical review of studies of polymeric seals in reciprocating hydraulic systems. Proceedings of the Institution of Mechanical Engineers, Part J: Journal of Engineering Tribology 213, 215-226.
Nijhof, J., Koloy, T.R., Andersen, K., 2010. Valhall - Pushing the limits for Open Hole Zonal Isolation - qualification and field trial of 10.000 psi oil swelling packers, SPE EUROPEC/EAGE Annual Conference and Exhibition. Society of Petroleum Engineers, Barcelona, Spain.
Nikas, G.K., 2003. Analytical study of the extrusion of rectangular elastomeric seals for linear hydraulic actuators. Proceedings of the Institution of Mechanical Engineers, Part J: Journal of Engineering Tribology 217, 365-373.
Parker, 2007. Parker O-Ring Handbook - ORD5700. Parker Hannifin Corporation, Cleveland, OH, USA.
Rivlin, R.S., Thomas, A.G., 1953. Rupture of rubber. I. Characteristic energy for tearing. Journal of Polymer Science 10, 291-318.
Rogers, W.P., Armstrong, N.A., Acheson, D.C., Covert, E.E., Feynman, R.P., Hotz, R.B., Kutyna, D.J., Ride, S.K., Rummel, R.W., Sutter, J.F., Arthur B. C. Walker, J., Wheelon, A.D., Yeager, C.E., 1986. Report of the Presidential Commission on the Space Shuttle Challenger Accident, Chapter IV: The Cause of the Accident, in: Commission, R. (Ed.).
She, S., Xu, C., Yin, X., Tong, W., Gao, C., 2012. Shape Deformation and Recovery of Multilayer Microcapsules after Being Squeezed through a Microchannel. Langmuir 28, 5010-5016.
Sun, J.-Y., Zhao, X., Illeperuma, W.R.K., Chaudhuri, O., Oh, K.H., Mooney, D.J., Vlassak, J.J., Suo, Z., 2012. Highly stretchable and tough hydrogels. Nature 489, 133-136.
Wang, Z., Liu, Q., Lou, Y., Jin, H., Suo, Z., 2015. Elastic Leak for a Better Seal. Journal of Applied Mechanics 82, 081010-081010.
Wyss, H.M., Franke, T., Mele, E., Weitz, D.A., 2010. Capillary micromechanics: Measuring the elasticity of microscopic soft objects. Soft Matter 6, 4550-4555.
Yakeley, S., Foster, T., Laflin, W.J., 2007. Swellable Packers for Well Fracturing and Stimulation, SPE Annual Technical Conference and Exhibition. Society of Petroleum Engineers, Anaheim, California, U.S.A.

Appendix A

Synthesis of hydrogels. We synthesize polyacrylamide hydrogels by free-radical polymerization. Acrylamide (AAM), N,N'-methylenebis(acrylamide) (MBAA), ammonium persulfate (APS) and N,N,N',N'-tetramethylethylenediamine (TEMED) are purchased from Sigma Aldrich. All materials are used as received. We dissolve powder of AAM in deionized water and add MBAA as the crosslinker in quantities specified in Table 1. We add TEMED as the accelerator and APS as the initiator in quantities of 0.0025 and 0.0085 times the weight of AAM. We color the hydrogel in red using a food dye (Shank's Extracts, purchased from VWR

International LLC.) in quantity of 0.002 times the volume of the aqueous solution. We pour the solution into acrylic molds to form rectangular samples. The samples are stored at room temperature for 1 day to complete polymerization.

Appendix B

Measurement of shear modulus and fracture energy. We measure the shear moduli and fracture energies of hydrogels by the pure shear test (Rivlin and Thomas, 1953; Sun et al., 2012). For a hydrogel of the same composition, we prepare three groups of samples to get the mean value and scatter of measured properties. Each group has two samples of the same dimensions. One sample is unnotched, and the other one is notched (Fig. B1). The samples are glued between two plastic gripers by using All Purpose Crazy Glue (purchased from VWR International LLC). In the undeformed state, each sample is of width $a_0 = 50$ mm, thickness $t_0 = 2$ mm, the length between two gripers is $L_0 = 10$ mm. The unnotched sample is used to measure the stress-stretch curve. The initial slope of the curve is the plane-strain modulus of the gel, $\bar{E}$. Compare to the modulus obtained from uniaxial tension, E,

$$\bar{E} = \frac{E}{1-\nu^2}, \tag{B1}$$

where ν is the Poisson's ratio. For incompressible material, $\nu = 0.5$, so that the shear modulus is related to the initial slope of the stress-strain curve as

$$\mu = \frac{E}{3} = \frac{\bar{E}}{4} = \frac{ds(\lambda = 1)}{4d\lambda}. \tag{B2}$$

When the sample is pulled to stretch λ, the area beneath the stress-stretch curve is the elastic energy density in the gel, $W(\lambda)$. The notched sample is prepared by cutting a crack with

$c_o = 20$ mm by a razor blade. The notched sample is used to measure the critical rupture stretch, λ_c, when the notch turns into a running crack. The fracture energy of the gel is given by

$$\Gamma = W(\lambda_c) L_o \tag{B3}$$

All the test results are summarized in Table 2. It should be pointed out that the fracture energy measured in experiments is for mode I cracks. However, it is unclear if the seals rupture exactly in mode I. Here we neglect possible mixed mode fracture and the dependence of the fracture energy on the mode mix. In comparing the theory and the experiment, we simply use the fracture energy for mode I cracks.

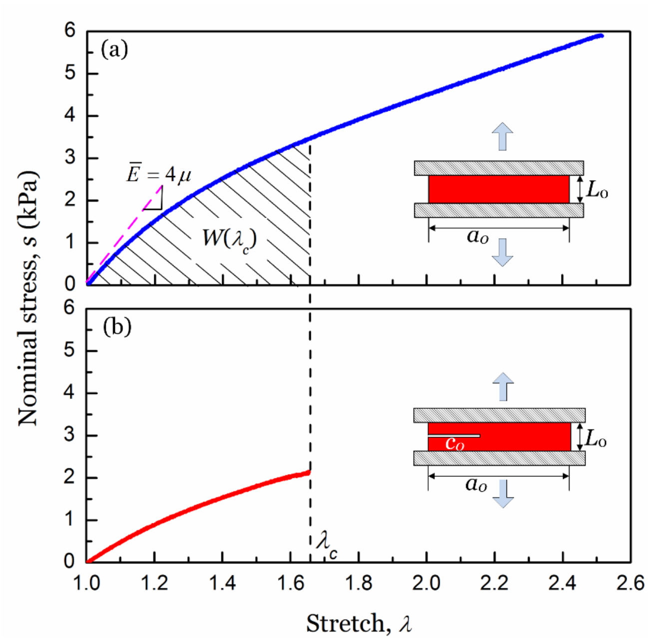

Fig. B1. Experimental determination of the shear modulus and fracture energy of a hydrogel. Two samples are pulled in tension. One sample is unnotched, and the other one is notched. (a) The unnotched sample is used to obtain the stress-stretch curve. The initial slope of the curve is the plane-strain modulus of the gel, $\bar{E} = 4\mu$. The area beneath the stress-stretch curve is the elastic energy density in the gel, $W(\lambda)$. (b) The notched sample is used to measure the critical rupture stretch, λ_c, when the notch turns into a running crack.

Appendix C

Measurement of sliding stress. We conduct an independent test on the sliding stress τ using a home-made setup (Fig. C1a). An acrylic plate is supported by four legs made of threaded studs and nuts. A bubble level is placed on the surface of acrylic plate to keep it horizontal by adjusting the location of the nuts. A hydrogel with dimensions $40\times40\times6$ mm is fully constrained by a stiff frame except the bottom surface is in contact with an acrylic sheet. There is a small gap about 1 mm between the frame and the surface of acrylic sheet to avoid their direct contact. Instead of precompression, here we place a weight on the frame to provide normal force on hydrogel. The hydrogel, the frame, and the weight are dragged horizontally by an Instron machine at a constant speed of 0.5mm/s and at a distance of 50mm.

The frictional stress is recorded as a function of the displacement measured at the moving part of the Instron machine (Fig. C1b). At small displacement, the string stretches and the hydrogel deforms, and the recorded stress increases. After the displacement is sufficiently large, the hydrogel slides steadily, and the recorded stress becomes nearly constant. We identify this constant stress as the sliding stress. When the weight is small (0.5 kg), The sliding stress fluctuates around the constant level. When the weight increases, the sliding stress increases slightly and then becomes nearly independent of the weight. The range of weights we put here is equivalent to the precompression (λ) around 0.5 to 0.9, which is comparable to what we used in sealing test. We determine the sliding stress for hydrogels of several values of elastic modulus (Fig. C1c).

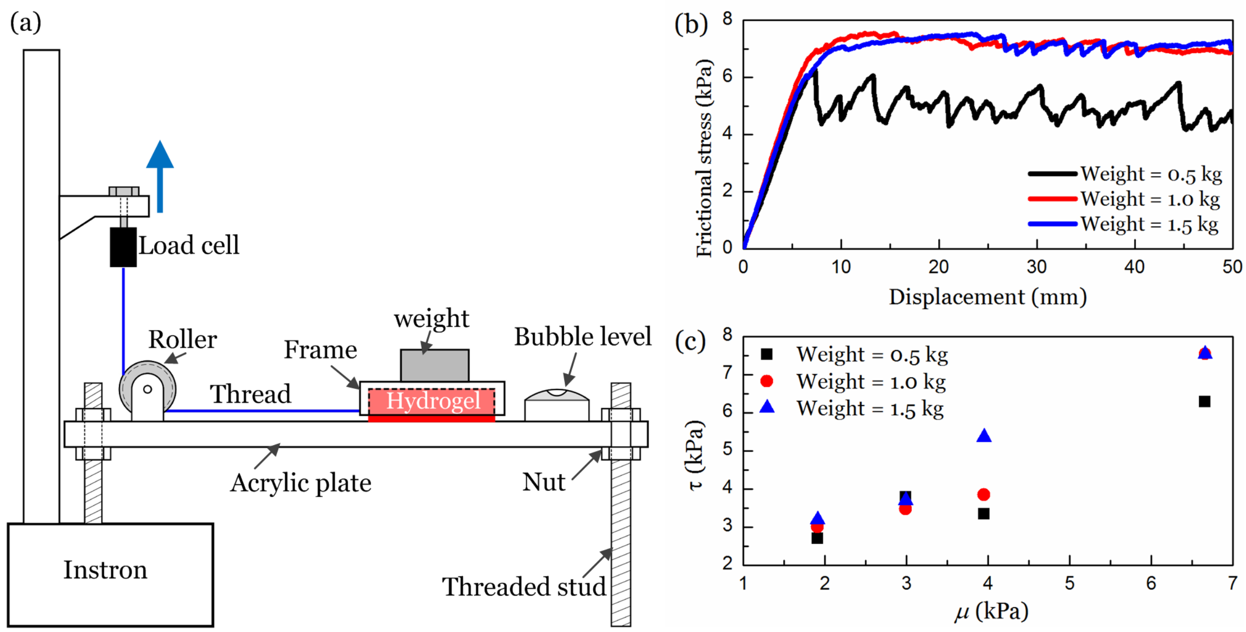

Fig. C1. Friction measurement by a customer-built set-up. (a) Experimental set-up. (b) frictional stress – displacement curve under different weights. The shear modulus is μ =6.6 kPa (M-88-06). (c) The relation between the frictional stress τ and the shear modulus μ .

Supplementary Information

Movie 1. As we inject water (colored blue) into the sealed chamber at a constant rate 2 ml/min. the pressure inside the chamber increases with time. When the fluid pressure is small, no obvious deformation of the seal (colored red) can be observed. When the pressure is high (beyond 40 kPa, i.e. 0.4 bar in the movie), the seal is pushed forward and the seal slides against the cover acrylic sheet.

Movie 2. As the fluid pressure reaches a critical value (85.7 kPa, i.e. 0.857 bar in the movie), a crack initiates at the front-bottom of the seal. Initially the crack grows slowly, then propagates across the length of the seal quickly. The fluid leaks through the crack, and the fluid pressure decreases to zero.